academicJournals

Vol. 9(15), pp. 339-349, 16 August, 2014
DOI: 10.5897/IJPS12.655
ISSN 1992 - 1950
Article Number: EF967E547019

http://www.academicjournals.org/IJPS

International Journal of Physical Sciences

Full Length Research Paper

Analysis and evaluation of differential inductive transducers for transforming physical parameters into usable output frequency signal

A. Deji, S. Khan*, M. M. Ahmed, J. Chebil and A. H. M. Z. Alam

Department of Electrical and Computer Engineering, International Islamic University, Malaysia.

Received 09 October, 2012; Accepted 3 June, 2013

This paper presents a novel hybrid oscillating inductive sensor circuit converting deflection oscillations into useful signal and thus being used to support an oscillatory circuit mechanism and management of their resulting oscillation in a real-time implementation. This circuit does not only detects and optimizes the deflections produced in an oscillation in instrumentation electronics, but also provide an improved sensory with high accuracy, sensitivity, responsiveness and operating range. The design therefore help in transforming the deflection deviations in the in and out movement of the core into useful output content. A simulation and derivation of the oscillating circuit in see-saw convulsion bar sensing system has been implemented. Simulation and derivations shows how the oscillating circuits of the bar are converted into frequency, duty cycle, current, voltages for further wireless applications.

Key words: Differential inductive sensing, displacement inductance-to-frequency converter, deflection deviation, see-saw bar, oscillation, position sensing.

INTRODUCTION

Sensors have proven important in converting immeasurable quantities such as wind velocity, vibrations, oscillation, turning effects of forces, deviations, illness etc into qualitative and quantitative electrical signal suitable for real time implementation by an intelligent oscillation harvesting mechanism. For an accurate measurement of such oscillation parameter, an efficient oscillation detector is essential (Figure 1).

This is capable of converting a see-saw convulsion bar into frequency response, duty cycle response, voltage response. The sensor output should be such that the oscillation/vibration, their motion, damping etc is determined. Based on the sensing inductive principle used, the designed circuit can be categorized into a vibration sensor and pressure sensor applied even in height location such as; sagging and oscillations of electrical transmission line, turning moment in railroad, signal upgrade from degradation in GSM mask (Ezzat and Cheng, 2011; Edgarcio et al., 1988; Grover and Deller, 1999; Hameed et al., 2012).

The sensor output should be such that electro-mechanical deviations in oscillation circuit and their effects servomechanism are determined. The vibration *sensor can be categorized according to the sensing* element such as resistive, capacitive, inductive and linear variable differential transducer (Mohammed et al., 2012;

*Corresponding author. E-mail: sheroz@iium.edu.my.

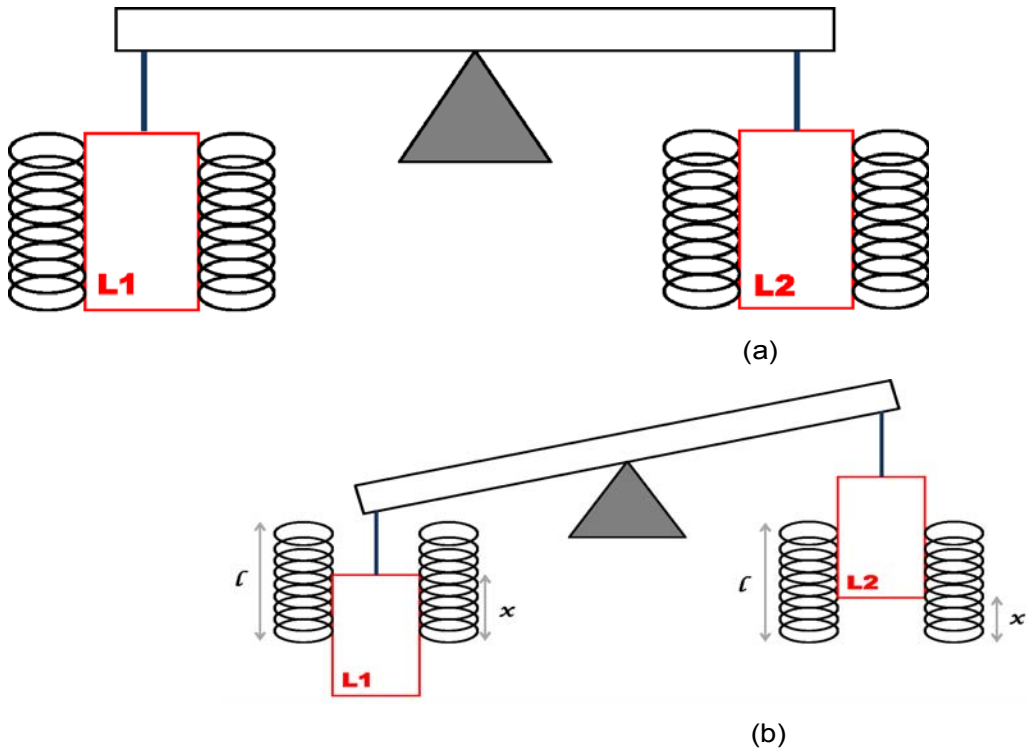

Figure 1. (a) A balance see-saw of overhanging bar, (b) Differential manner of an overhanging see-saw bar.

Mohan et al., 2008). Piezo-resistive sensors have good linearity and acceptable sensitivity, but suffer from the problem of inaccuracies (Mohan et al., 2009; Ravindra, 2006). Capacitive pressure/oscillation sensors exhibit features of higher sensitivity and lower temperature hysteresis, but they are usually nonlinear (Ravindra, 2006; Saxena and Sahu, 1994; Slamwomir, 2007). Conventional LVDT-based pressure/oscillation sensors possess good linearity, highest sensitivity and lowest temperature hysteresis, but such devices have got bulky physical structures (Saxena and Sahu, 1994; Slamwomir, 2007; Texas Instruments, "LM555 Data sheet", 2003; Udaya and Duleepa, 2011). This paper presents a sensor capable of harnessing oscillations in circuits into pulse able signal. Each aspect of this finding has been put into different sections.

STRUCTURAL MODEL AND DESIGN

The structure of the proposed oscillating circuit is shown schematically in Figure 2. The oscillation of the actual component of the sensor varying differentially, maximizing the circuit variations and deviations into a derivable and pulse able signal is shown in Figure 3. As shown in Figures 2, 3 and 4, a vertical core of a varying height of 4 to 36 mm is embedded into an open stator made up of magnetic coils thereby providing the inductive change in relation to circuit vibrations. The oscillation of the circuit provides the force or pressure needed to bring about the inductance of the coil as the core is displaced in and out of the coils mounted in a stator of a servomechanism. This displacement is proportional to the force or pressure and the inductance of the core. The timer circuit when connected to the coils in Figures 1 and 2 will give rise to Figures 3 and 4. This RL3R circuit gives us a square wave with a frequency depending on the inductance value of the coil as shown in Figure 5.

MATHEMATICAL MODEL OF THE CIRCUIT

A differential transducer is one that simultaneously senses two separate sources and provides an output proportional to the difference between the sensing. Considering the idea in Figure 4, the inductances of the two coils change in a differential manner when the overhanging bar is moving in a seesaw manner. At position '*x*', the inductance of the right hand side of the coil is given by Equation (1), while that of the left hand side is given by Equation (2), giving the total equation as follows:

$$L_{TOTAL} = \frac{\mu_0 N^2 A}{l}\left[\mu_r \frac{x}{l} + \frac{l-x}{l}\right] = \frac{\mu_0 N^2 A}{l}\left[1 + \frac{x}{l}(\mu_r - 1)\right] \quad (1)$$

$$L_{TOTAL} = \frac{\mu_0 N^2 A}{l}\left[\frac{x}{l} + \mu_r\left(\frac{l-x}{l}\right)\right] = \frac{\mu_0 N^2 A}{l}\left[\mu_r + \frac{x}{l}(1-\mu_r)\right] \quad (2)$$

Details of the derivation of equation 1 and 2 are shown in the APPENDIX A-1 to A-6. A linear relationship is shown in Figure 6 demonstrating the in and out oscillation of the device.

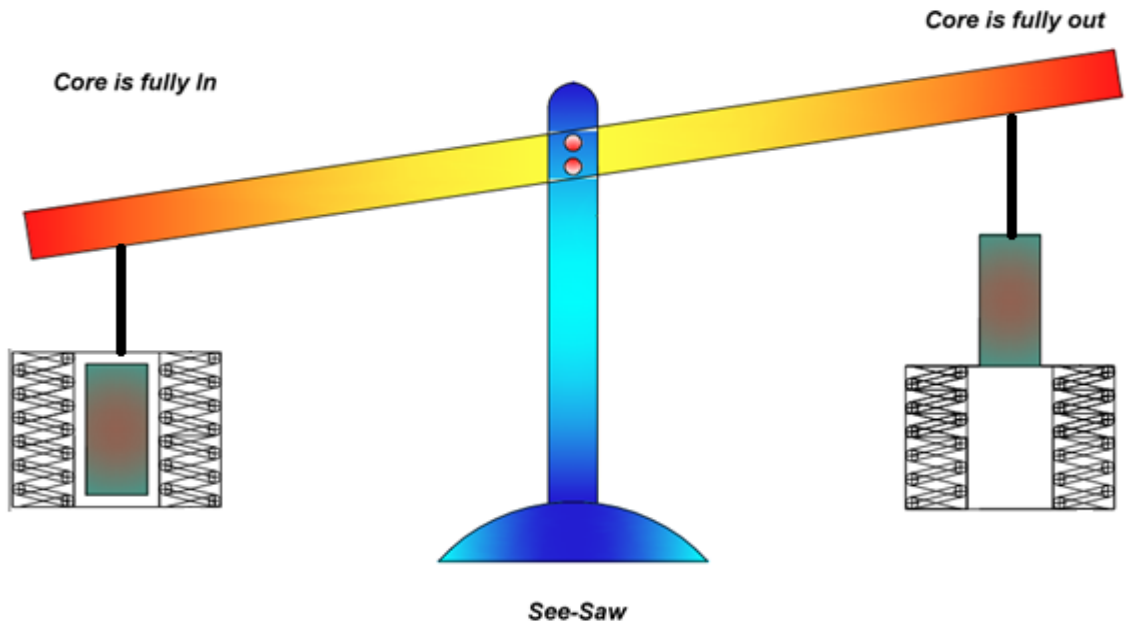

Figure 2. Varying differential cores in a see-saw.

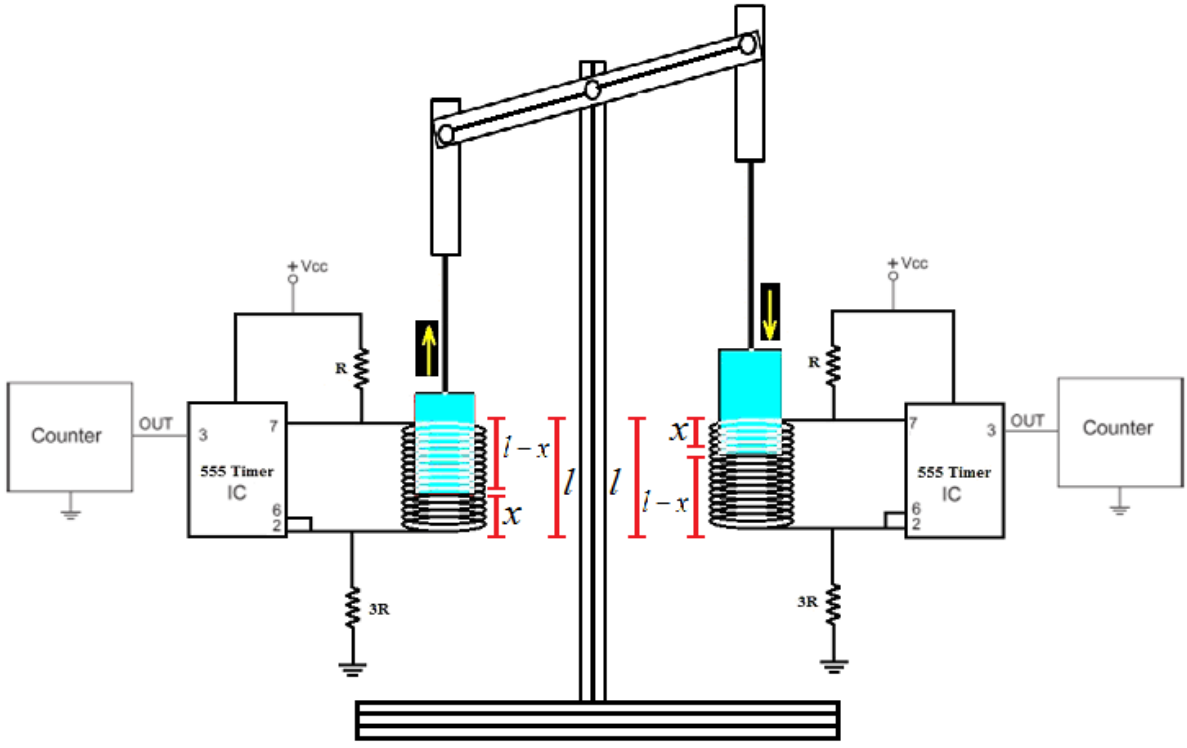

Figure 3. Differential inductive system architecture.

Frequency output for inductive change delta L

The inductance of left inductor is given by L_1 and can be expressed as:

$L_1=L_{fi}-\Delta L_1$

$\Delta L_1=L_{fi}-L_1$

Whereas the inductance of second inductor is given by L_2

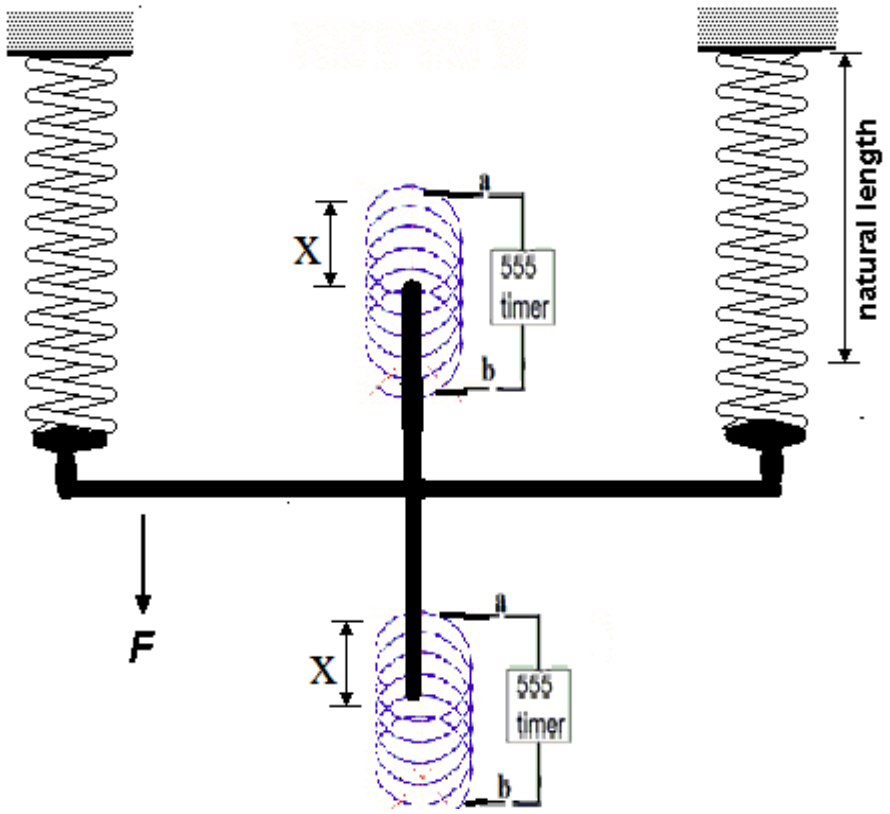

Figure 4. Signal produced from circuit oscillation and vibrations.

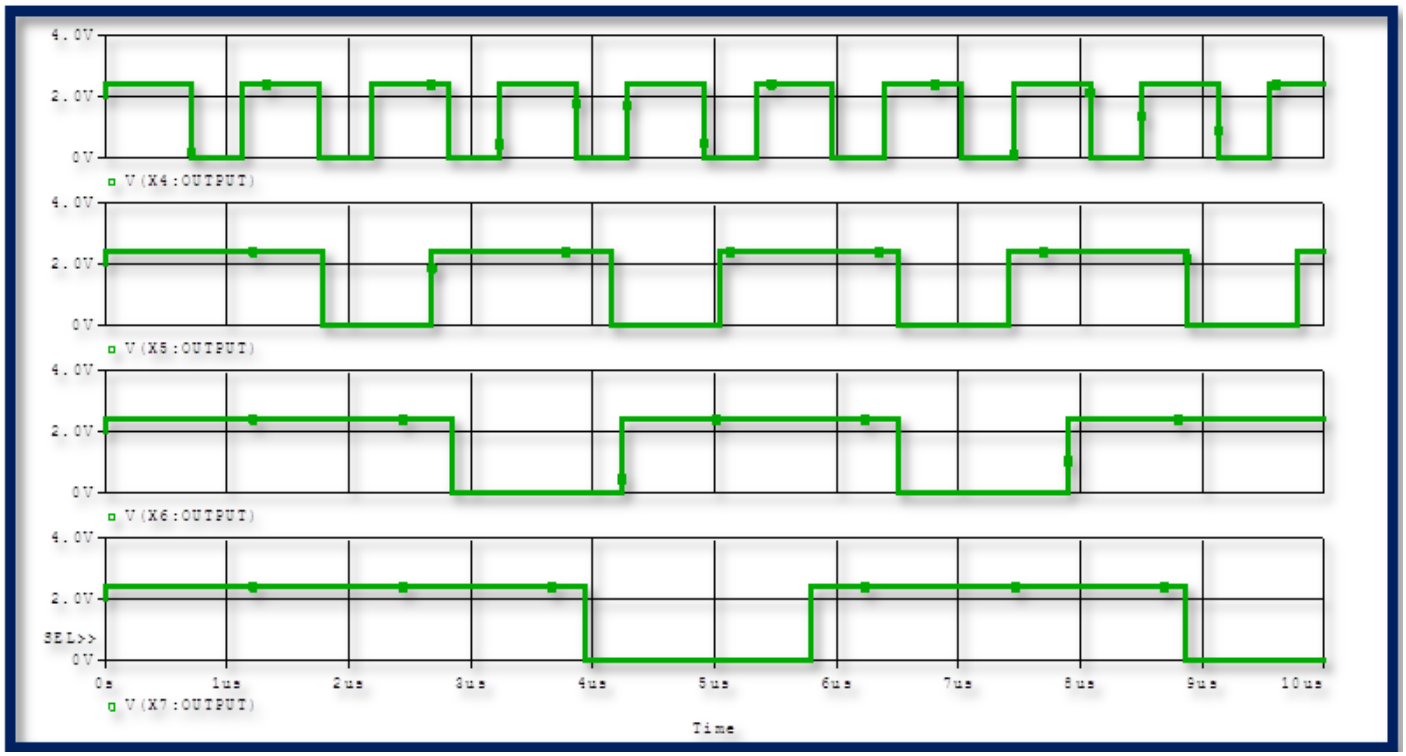

Figure 5. Voltage waveform from circuit oscillation.

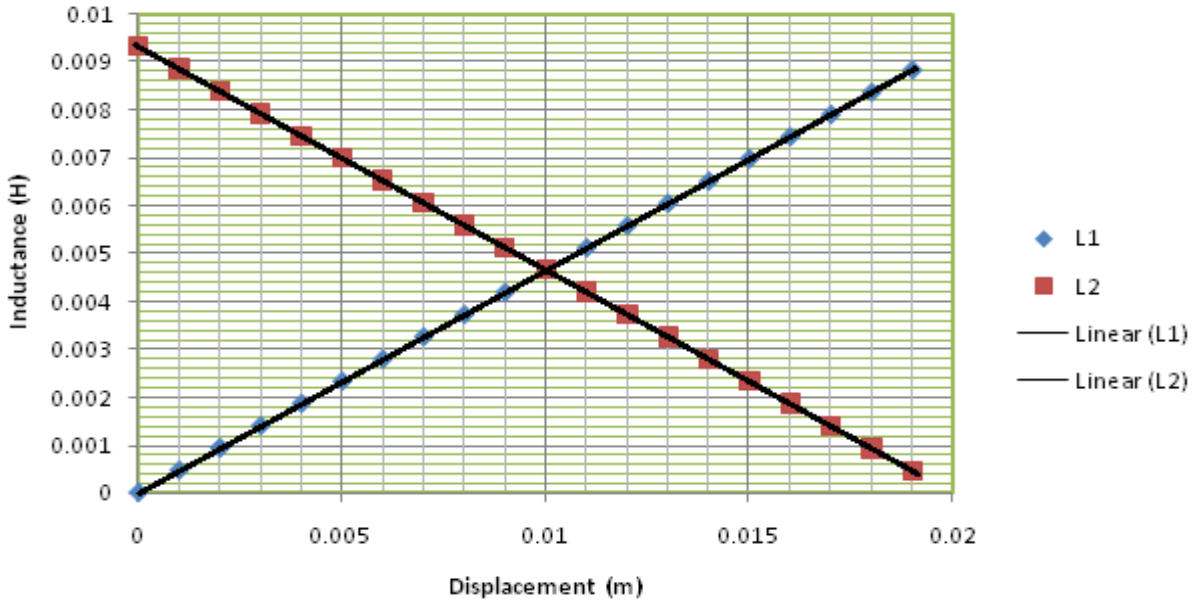

Figure 6. A plot of the inductance variation with the displacement.

$L_2=L_{fo}+\Delta L_2$

$\Delta L_2=L_2-L_{fo}$

$\Delta L_{avg}=\frac{\Delta L_1+\Delta L_2}{2}$

The frequency of RL3R-timer circuit for single inductor is given by:

$$f=1.58\frac{R}{L}$$

The frequency of the first inductor is:

$$f_1=1.58\frac{R}{L_{f1}-\Delta L_1} \quad (3)$$

The frequency of the second inductor is:

$$f_2=1.58\frac{R}{L_{fo}+\Delta L_2} \quad (4)$$

The frequency of total inductive change is:

$$\Delta f_1 = f_1 - f_{f1} = 1.58R\left(\frac{1}{L_1}-\frac{1}{L_{f1}}\right) \quad (5)$$

$$\Delta f_1 = 1.58R\left(\frac{L_{f1}-L_1}{L_1L_{f1}}\right) = 1.58R\left(\frac{\Delta L1}{L_1L_{f1}}\right)$$

Substituting the value of L_1 in Equation (5) we get:

$$\Delta f_1 = 1.58R\left(\frac{\Delta L_1}{(L_{f1}-\Delta L_1)L_{f1}}\right) \quad (6)$$

Now solving for the other case of Δf_2, we obtain;

$$\Delta f_2 = f_{f2} - f_2 = 1.58R\left(\frac{1}{L_{f2}}-\frac{1}{L_2}\right) \quad (7)$$

$$\Delta f_2 = 1.58R\left(\frac{L_2-L_{f2}}{L_2L_{f2}}\right) = 1.58R\left(\frac{\Delta L_2}{L_2L_{f2}}\right) \quad (8)$$

Substituting the value of L_2 in Equation (7),

$$\Delta f_2 = 1.58R\left(\frac{\Delta L_2}{(L_{f2}-\Delta L_2)L_{f2}}\right) \quad (9)$$

$$\Delta f_{in/r} = \frac{\Delta L_1+\Delta L_2}{2} \quad (10)$$

The plot for frequencies of the in and out movement of the core in the coil is given thus.

Frequency change as a function of displacement

From the previous equation, the frequency change as a function of displacement is given thus as:

$$\Delta f_1 = 1.58R\left(\frac{I^2}{\mu_o N^2 A[1+x(\mu_r-1)]} \quad \frac{1}{L_{f1}}\right) \quad (11)$$

That of the second coil is;

$$\Delta f_2 = 1.58R\left(\frac{1}{L_{f2}} - \frac{I^2}{\mu_o N^2 A[\mu_r \ln x(1-\mu_r)]}\right) \quad (12)$$

The plot for frequencies of the in and out movement of the core in the coil is given as; these change in frequencies from Equations (11) and (12), gives a symmetrical behaviour with respect to the displacement produced by the oscillatory motion of the core. This aforementioned behaviour gave rise the plot in Figure 7(a) showing the reciprocal behaviour of the in and out movement, harnessing the deviations in terms of oscillation in servomechanism and electro-mechanical devices. The frequency change with the displacement is given in Figure 7(b).

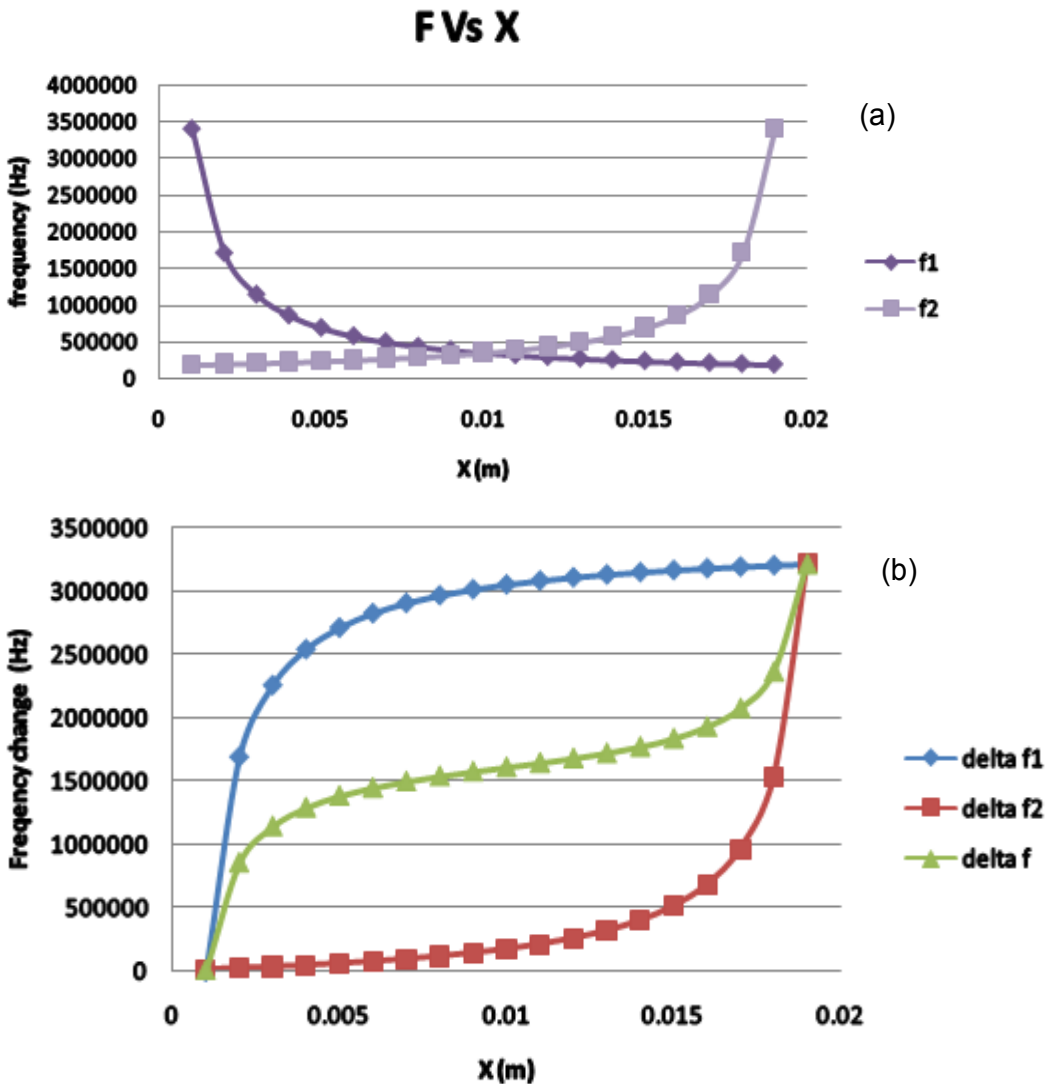

Figure 7. (a): A plot of Frequency change in symmetrical variation with respect to core displacement, (b): A plot of Frequency with respect to core displacement.

Frequency as a function of oscillations

Generally, vibrations in movement can be described or expressed by the following equations. In the case the seesaw bar shown in Figures 2 through 4, we assume that the seesaw bar in the springs has a movement which is a simple harmonic motion according to the following equation;

$$X = 0.5l - a.5l\cos(2\pi f_s t) \quad (13)$$

The vibrations found in electronic circuit and in machines can be converted into useful frequencies as shown in Equations 14 and 15.

$$f_1 = \frac{1.25R^2}{\mu_o N^2 A[1+(0.5l - a.5l\cos(2\pi f_s t))(\mu_r - 1)]} \quad (14)$$

$$f_2 = \frac{1.25R^2}{\mu_o N^2 A[\mu_r[1+(0.5l - a.5l\cos(2\pi f_s t))(\mu_r - 1)]} \quad (15)$$

To check the effect of the sea saw bar frequency, Equations (13), (14) and (15) are used. Assuming a coil of length of 20 mm, number of turns = 100, cross sectional area A=pi(r*r) where r=1 mm, an iron core with relative permeability 4728, and R= 1k ohm, then by changing the value of fs, the plots for the output frequency as a measure of x is obtained. Figure 8 shows the effect of the circuit as it oscillates, converting the deviations into these useful frequency values when the harmonics from the see-saw in the convulsion are given as 10, 100, 1000 and 10,000 Hz respectively.

SIMULATION RESULT AND ANALYSIS

A simulation of the designed mathematical model and its necessary derivations for frequency, frequency hysteresis, voltage and the current responses are carried out. The results obtained confirm the mathematical derivation plots with the simulation. Figure 9(a) is the

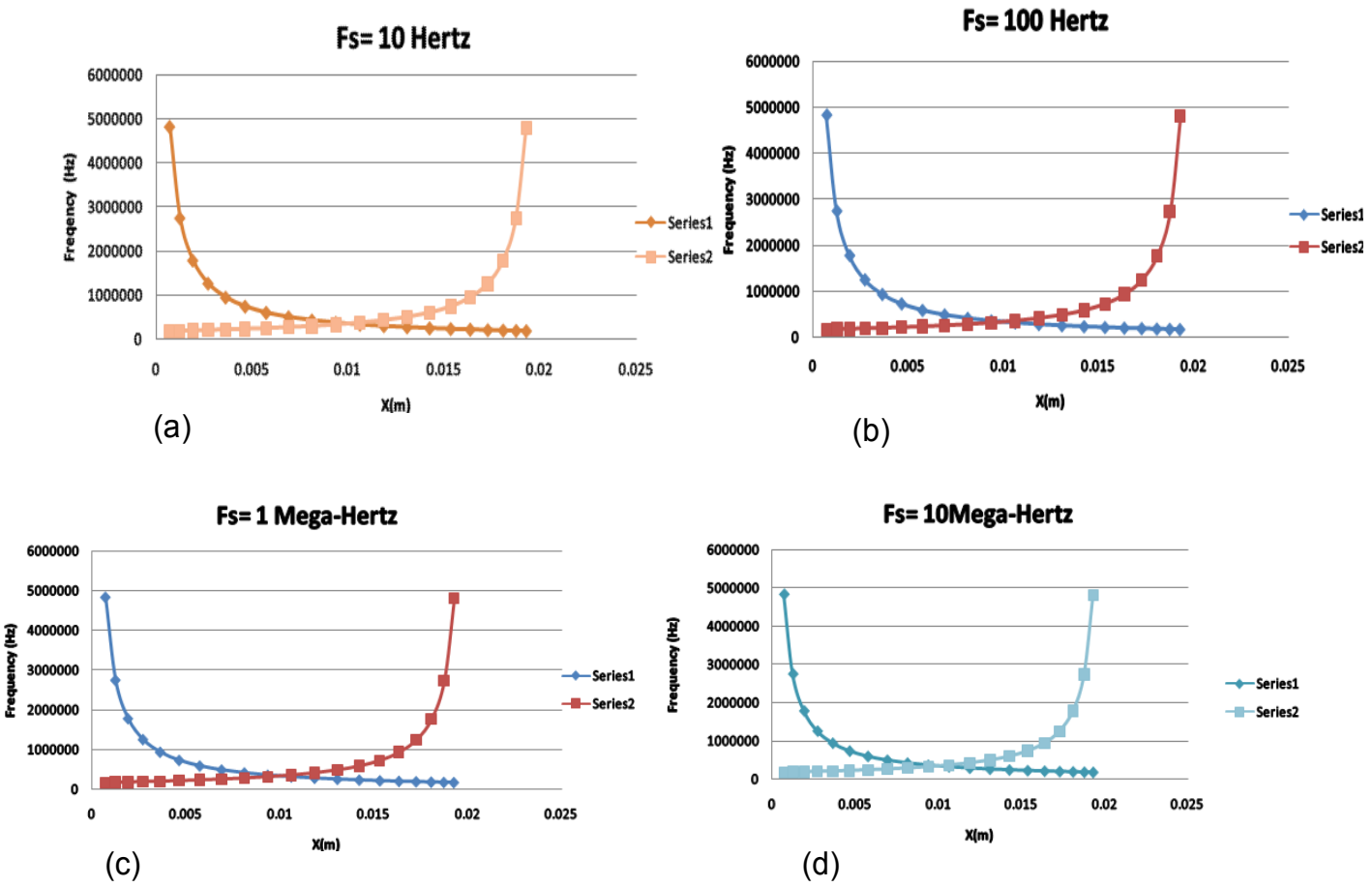

Figure 8. Plot of the Output Response for oscillating circuit for varying values of Fs.

result of simulation of both circuits; the right and the left one using the same assumption that was used in the calculations. The green line represents the frequency output of the left side and the red one is for the circuit in the right hand side as a measure of the core displacement. Figure 9(b) shows the output frequency when the sea saw frequency fs= 100 Hz, for three time periods, in every period, the displacement value change from 0 to l and from l to 0.

Figure 10(a) to (d) shows the result of simulation when the sea saw bar frequency is change. When the frequency of sea saw bar is 10 Hz, x changes from 0 to l, and time t, is changed from 0 to 50 ms, 0 to 100 ms, 0 to 1000 ms and 0 to 10000 ms according to Equation (15). The results obtained confirm those of the derivations shown in this work. A slight difference in simulation analytical deduction is due to the environmental effect on the circuit. The table for the different frequencies giving rise to frequency hysteresis is given in Table 1. This table gives rise to Figure 6, showing the frequencies of the see-saw behavior when the core is differentially in and out of its coil as the circuit oscillate.

A linear relationship exist between the inductance of the first coil, which increases when the core is moving in, while the core for the second coil is moving out, with decrease in inductance. The inductance change ΔL is calculated and plotted in Figure 6. These inductance change leads to a frequency change and hysteresis for the output of the timers as seen from derivations and simulation results. This shows that the frequency is decreasing when the core is going in and increases when the core goes out. At equilibrium state when the sea saw bar is horizontal, the displacement x is equal to half of the coil length, l and the value of the inductance for both coils is the same. This is clearly shown in Figure 6 at the point when x= 10 mm, the inductance L=4.67 mH for the two coils. The result of the inductance equality at this point is reflected to the frequency value as Figure 7.

The main difference between derivations and simulation result is seen when the coil is almost fully out. From derivation point, when the coil is fully out x=0, the frequency is larger than 800 Mega Hz, which is very large compared to other frequency values which ranges from 0.18 to 3.4 Mega Hz. On the other hand, simulation result

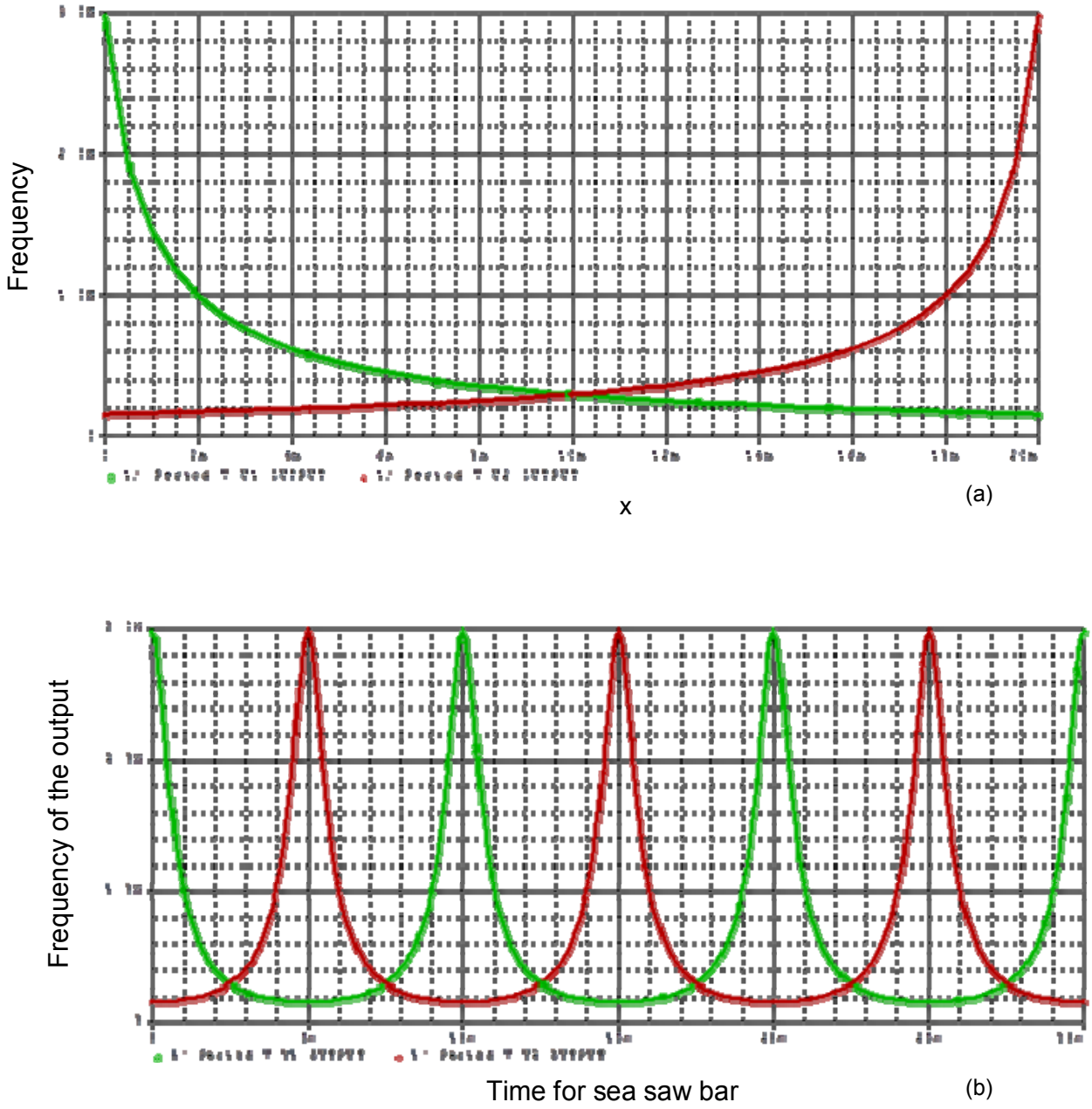

Figure 9. (a): A simulation of Frequency change in symmetrical variation with respect to core displacement, (b): Simulated Output for frequency with three time periods.

shows that maximum frequency occurs when the core is fully out and this is at 3 MHz as shown Figure 7. Although, the result from derivations and simulation has shown that the sea saw bar frequency has no effect on the output frequency values, the frequency counter calculate the value which is equal to the time period of the timer output for every reading. So, if the sea saw frequency fs exceeds a certain value, the frequency counter will give wrong frequency output. This value is derived as shown in Equation (16).

$$\sum_{x=0}^{x} 0.63 \frac{\mu_0 N^2 A}{R l^2}\left(l + x(\mu_r - 1)\right) \quad (16)$$

Conclusion

Differential sensing system architecture is proposed as shown in Figures 1 to 4. This consists of two coils with varying cores in which a change in the core position will result in inductance change. These changes can be

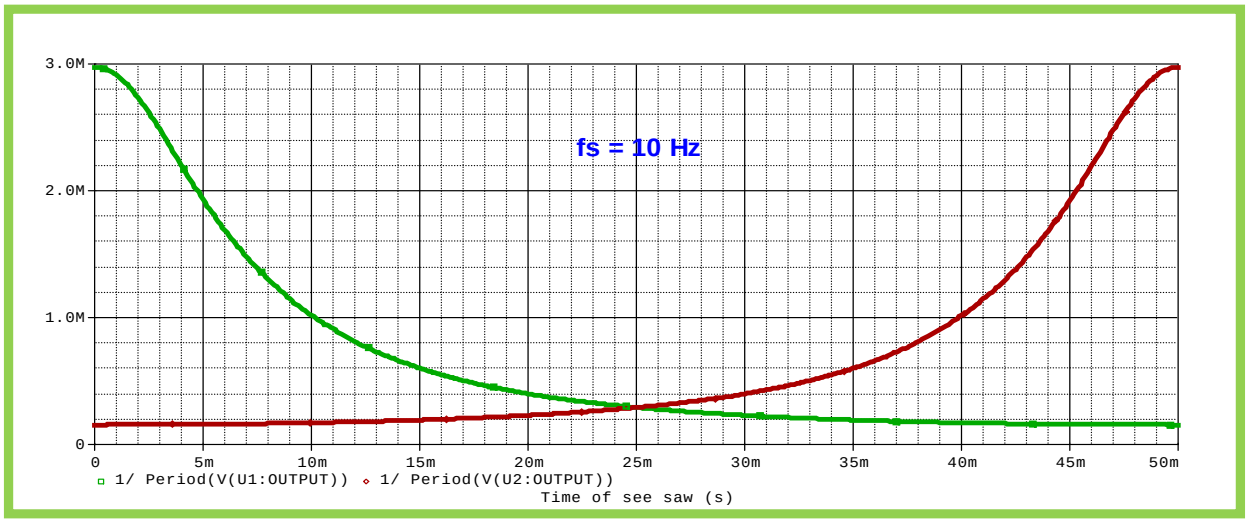

(a)

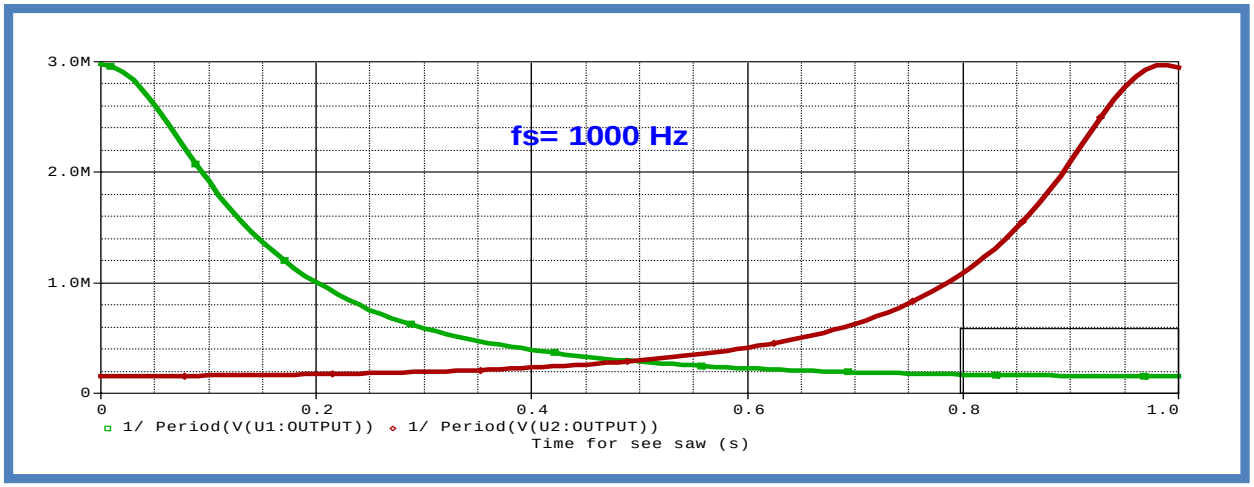

(b)

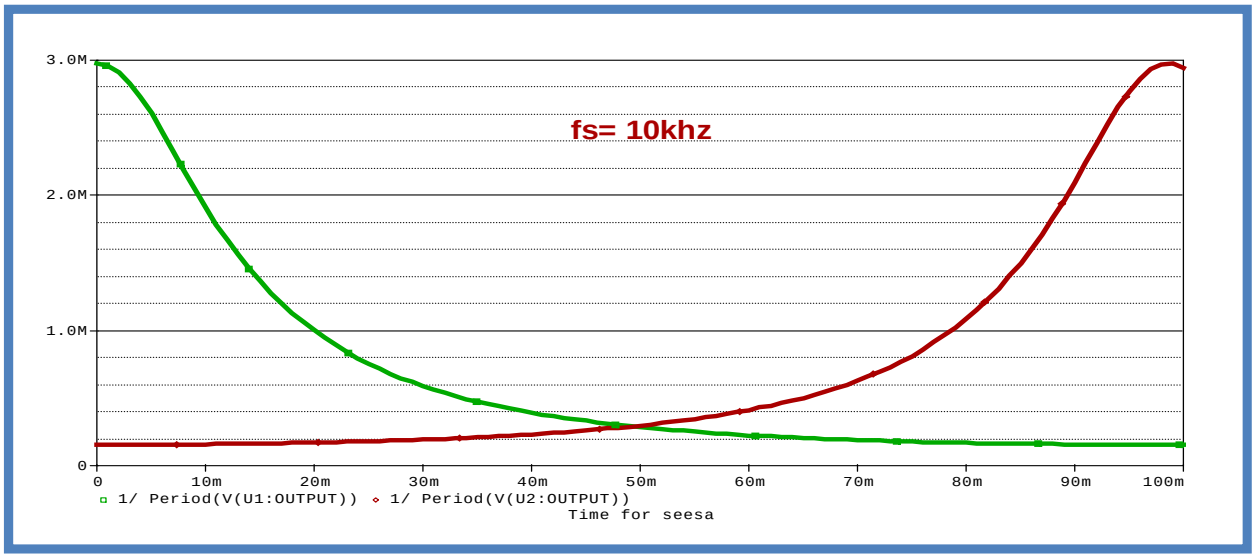

(c)

Figure 10 (a-d): Simulation values for different harmonics in the see-saw.

Table 1. Simulation details of frequency hysteresis.

X	delta f1	delta f2	delta f
0.001	0.109400729	8958.646289	4479.3778
0.002	1692127.847	18912.4638	855520.16
0.003	2257759.167	30037.02729	1143898.1
0.004	2540873.66	42551.79359	1291712.7
0.005	2710838.104	56734.72486	1383786.4
0.006	2824187.656	72943.17702	1448565.4
0.007	2905171.185	91644.4259	1498407.8
0.008	2965919.533	113461.451	1539690.5
0.009	3013174.592	139243.6828	1576209.1
0.01	3050982.636	170180.1802	1610581.4
0.011	3081919.134	207988.2244	1644953.7
0.012	3107701.365	255243.2833	1681472.3
0.013	3129518.39	315991.6318	1722755
0.014	3148219.639	396975.1606	1772597.4
0.015	3164428.091	510324.7128	1837376.4
0.016	3178611.023	680289.1565	1929450.1
0.017	3191125.789	963403.6494	2077264.7
0.018	3202250.353	1529034.969	2365642.7
0.019	3212204.17	3221162.707	3216683.4

converted into frequency output in the processing part of the sensor using a timer circuit. Simulation of the proposed system shows a similar result with that of theoretical derivation. The sea saw bar frequency effect is checked and the limitation for this value. This was found in Equation (16). Finally, this novel design provides a platform for electro-mechanical and servomechanism system deviation in form of oscillation and vibration to be harvested into useful electrical signal by the help of designed differential inductive sensor using both coils transducers as shown in Figure 3. The result obtained appears to be at minimum value of 0.001% of FSO which serve as improvement and introduction frequency hysteresis results in both derivations and in simulations.

Conflict of Interest

The authors have not declared any conflict of interest.

REFERENCES

Ezzat G, Cheng HMM (2011). “High-Sensitivity Inductive Pressure Sensor,” IEEE Trans. Instrum. Meas. 60(8).

Edgarcio AB, Caballero WU, Aldonate J (1988). “Inductive Proximity Transducer”, IEEE Engineering in Medicine & Biology Society 10th Annual International Conference.

Grover D, Deller JR (1999).‘Digital Signal Processing And The Microcontroller, chapter 2, Motorola University Press - Prentice Hall Professional Technical Reference, Upper Saddle River, NJ. pp. 15-20.

Hameed SA, Aboaba A, Khalifa AA, Abdalla OO, Daoud AH, Saeed JI, Mahmoud RA (2012). Framework for enhancement of image guided surgery: Finding area of tumor volume, Aust. J. Basic Appl. Sci. 6(1):9-16. (ISI Cited publication).

Mohammed SS, George AB, Vanajakshi L, Venkatraman J (2012). “A Multiple Inductive Loop Vehicle Detection System for Heterogeneous and Lane-Less Traffic,” IEEE Trans. Instrum. Meas. 61(5):1353-1361. http://dx.doi.org/10.1109/TIM.2011.2175037

Mohan NM, Shet AR, Kedarnath S, Kumar VJ (2008). “Digital Converter for Differential Capacitive Sensors,” IEEE Trans. Instrum. Meas. 57(11):2576-2581. http://dx.doi.org/10.1109/TIM.2008.922109

Mohan NM, George AB, Kumar VJ (2009). “Analysis of a Sigma–Delta Resistance-to-Digital Converter for Differential Resistive Sensors,” IEEE Trans. Instrum. Meas. 58(5):1617-1622. http://dx.doi.org/10.1109/TIM.2009.2012949

Ravindra W (2006). ‘Inductive Fiber-Meshed Strain and Displacement Transducers for Respiratory Measuring Systems and Motion Capturing Systems’ IEEE Sensors J. 6(3).

Saxena SC, Sahu C (1994). “Differential Inductive Ratio Transducer with Short-circuiting Ring for Displacement Measurement”, IEEE Trans. Instrum. Meas. 43(5). http://dx.doi.org/10.1109/19.328885

Slamwomir T (2007). “Induction Coil Sensors-a review. Institute of Electrical Theory and Measurement”, UlKoszykowa 75,00-661 Warsaw, Poland, pp. 31-46.

LM555 Data sheet (2003). Texas Instruments.

Udaya KM, Duleepa JT (2011). “A Bidirectional Inductive Power Interface for Electric Vehicles in V2G Systems,” IEEE Trans. Ind. Elect. 58(10): 4789-4796. http://dx.doi.org/10.1109/TIE.2011.2114312

Appendix 1

Inductance of the part containing the core L_1 is given as:

$$L_1 = \frac{\mu_r \mu_0 N_1^2 A}{l - x} \quad \text{(A-1)}$$

The inductance of the part with no core L_2 is given as:

$$L_2 = \frac{\mu_0 N_2^2 A}{x} \quad \text{(A-2)}$$

The numbers of turns in the first and second inductors above the total number of the coil under consideration give by

$$N = N_1 + N_2 \quad \text{(A-3)}$$

And, therefore, we know that

$$\frac{N_2}{N} = \frac{x}{l} N = \frac{Nx}{l}$$

Similarly;

$$N_1 = \frac{N(l-x)}{l} = N\left(1 - \frac{x}{l}\right) \quad \text{(A-4)}$$

Substituting the values of N_1 and N_2 into equations above:

$$L_1 = \frac{\mu_r \mu_0 N^2 \left(1 - \frac{x}{l}\right)^2 A}{l - x} = \frac{\mu_r \mu_0 N^2 A (l-x)}{l^2} \quad \text{(A-5)}$$

$$L_2 = \frac{\mu_0 N^2 \left(\frac{x}{l}\right)^2 A}{x} = \frac{\mu_0 N^2 A x}{l^2} \quad \text{(A-6)}$$

The total inductance is the series sum of the individual inductances L_1 and L_2, given as:

$$L = L_1 + L_2 \quad \text{(A-7)}$$